

RESEARCH ARTICLE

10.1002/2015JA021353

Key Points:

- Reference curves are not used anymore
- Larger earthquakes are preceded by larger precursors
- Precursors of larger earthquakes start earlier

Supporting Information:

- Figures S1–S6

Correspondence to:

K. Heki,
heki@mail.sci.hokudai.ac.jp

Citation:

Heki, K., and Y. Enomoto (2015), M_w dependence of the preseismic ionospheric electron enhancements, *J. Geophys. Res. Space Physics*, 120, 7006–7020, doi:10.1002/2015JA021353.

Received 21 APR 2015

Accepted 20 JUL 2015

Accepted article online 24 JUL 2015

Published online 19 AUG 2015

M_w dependence of the preseismic ionospheric electron enhancements

K. Heki¹ and Y. Enomoto²¹Department of Earth and Planetary Sciences, Hokkaido University, Sapporo, Japan, ²SASTec, Shinshu University, Nagano, Japan

Abstract Ionospheric electron enhancement was reported to have occurred ~40 min before the 2011 Tohoku-oki (M_w 9.0) earthquake, Japan, by observing total electron content (TEC) with Global Navigation Satellite Systems receivers. Their reality has been repeatedly questioned due mainly to the ambiguity in the derivation of the reference TEC curves from which anomalies are defined. Here we propose a numerical approach, based on Akaike's information criterion, to detect positive breaks (sudden increase of TEC rate) in the vertical TEC time series without using reference curves. We demonstrate that such breaks are detected 25–80 min before the eight recent large earthquakes with moment magnitudes (M_w) of 8.2–9.2. The amounts of precursory rate changes were found to depend upon background TEC as well as M_w . The precursor times also showed M_w dependence, and the precursors of intraplate earthquakes tend to start earlier than interplate earthquakes. We also performed the same analyses during periods without earthquakes to evaluate the usefulness of TEC observations for short-term earthquake prediction.

1. Introduction: History of Debate

Heki [2011] reported the enhancement of ionospheric electrons starting ~40 min before the 2011 M_w 9.0 Tohoku-oki earthquake, Japan, by observing the ionospheric total electron content (TEC) using the nationwide dense network of continuous Global Navigation Satellite Systems (GNSS) stations. Heki [2011] also found that similar enhancements preceded major earthquakes including the 2004 Sumatra-Andaman earthquake (M_w 9.2), the 2010 Central Chile (Maule) earthquake (M_w 8.8), and the 1994 Hokkaido-Toho-Oki earthquake (M_w 8.3). Later, Cahyadi and Heki [2013] reported that the 2007 South Sumatra (Bengkulu) earthquake (M_w 8.5) showed a similar enhancement, but plasma bubble activities made it difficult to find them before the 2005 Nias earthquake (M_w 8.6). In these studies, reference curves are defined to model the slant TEC (STEC) time series, and the anomalies were defined as the departure from these curves.

The reality of preseismic electron enhancements has been questioned by Kamogawa and Kakinami [2013]. They considered the enhancements an artifact that popped up by wrongly assuming the reference curves for time series including sudden drops due to electron depletions associated with coseismic subsidence of the surface [Kakinami et al., 2012; Shinagawa et al., 2013]. Heki and Enomoto [2013], in a rebuttal paper, demonstrated the reality of the preseismic enhancement in several ways. At first, they proposed to use absolute vertical TEC (VTEC) time series, which are free from apparent U-shaped changes seen in STEC, for better intuitive recognition of the phenomena. Using absolute VTEC, they demonstrated that preseismic increase and coseismic drops are similar in magnitude (their Figures 2 and 3). They also compared the VTEC data with those of other sensors (ionosonde and geomagnetic field) and showed that they started to change simultaneously [Heki and Enomoto, 2013, Figure 4].

Concerning the geomagnetic declination change that started ~40 min before the earthquake (i.e., ~05:00 UT), Utada and Shimizu [2014] commented that their spatial pattern suggests its space weather origin. Indeed, a larger geomagnetic declination change, clearly induced by a geomagnetic storm, occurred ~16 h later on the same day (~21:00 UT). In the reply, Heki and Enomoto [2014] pointed out two major differences between the 05:00 UT and 21:00 UT episodes. The first difference is their spatial distribution (anomalies are stronger in more northerly stations in the second episode, while this was not clear in the first). As the second difference, we showed that the second episode little influenced ionospheric TEC above NE Japan. Hence, even if the declination changes at ~05:00 UT is caused by a geomagnetic storm, the claim by Utada and Shimizu [2014] that the preseismic TEC increase is due to a storm would not be justified.

Masci et al. [2015], the latest objection article, doubted the reality of the preseismic electron enhancements based on their original analyses of the same STEC time series as in Heki [2011] (they did not give a reason why

they did not use absolute VTEC). Their criticisms half overlap with *Kamogawa and Kakinami* [2013]; they pointed out the ambiguity in defining the reference TEC curves (Criticism #1). They also showed that natural variability exceeds the preseismic anomalies (a figure similar to Figures 6b–6d of *Heki and Enomoto* [2013] is given) (Criticism #2). They considered it unnatural and wrong that all the reported preseismic electron enhancement started ~40 min before earthquakes in spite of the diversity in earthquake magnitudes and mechanisms (Criticism #3). They commented on the geomagnetic field and thought it unlikely that the preseismic anomaly ~40 min before the Tohoku-oki earthquake is seen only in the declination time series (Criticism #4).

The present paper is basically written as the direct rebuttal to *Masci et al.* [2015] but will also serve as a report of a few new findings, including the dependence of the size and time of the precursors on M_w and types of the earthquakes. As the response to Criticism #1, we will propose a new approach to identify “breaks” (abrupt increase in rate) in absolute VTEC time series as a substitute for the reference curves (section 2.3). Criticisms #3 and #4 seem to come from misunderstandings by *Masci et al.* [2015]. In section 3.3, we show that the onset time varies from 80 min (2004 Sumatra-Andaman) to 25 min (2014 Iquique) before earthquakes, and they depend on M_w and earthquake types. In section 4.3, we demonstrate that the breaks are found ~40 min before the 2011 Tohoku-oki earthquake in all the three components of the geomagnetic field

Rebuttal to Criticism #2 is not straightforward because we agree that the natural variability overwhelms the precursors in terms of amplitudes especially when geomagnetic activity is high. In this paper, we try to evaluate how often VTEC shows significant positive breaks similar to the preseismic ones. Then, we disprove the possibility that the occurrence of preseismic TEC breaks is a fortuitous coincidence. We will also try to clarify the characteristics of space weather origin VTEC changes, e.g., their propagation properties.

2. Data and Method: Absolute VTEC and Break Detection

2.1. STEC and the Reference Curve Method

At first, we emphasize the benefit of plotting absolute VTEC to interpret the net increase and decrease of ionospheric electrons. *Heki* [2011] modeled the STEC time series with the equation

$$\text{STEC}(t, \zeta) = \text{VTEC}(t) / \cos \zeta + B, \quad (1)$$

where ζ is the incident angle of the line of sight to the ionosphere and absolute VTEC is assumed to obey a polynomial of time t , i.e.,

$$\text{VTEC}(t) = \sum_{i=0}^m a_i t^i. \quad (2)$$

The bias B is inherent to phase observables of GNSS and remains constant for individual satellites in the studied period. *Heki* [2011] assumed cubic functions for VTEC ($m = 3$) and estimated the coefficients a_0 , a_1 , a_2 , a_3 , and B together in a single least squares run. There, time intervals possibly influenced by TEC disturbances before and after earthquakes were excluded. This “excluded time interval” is taken typically from 40 min before earthquakes to 20 min after earthquakes. Then the anomaly was derived as the departure of the observed STEC from the estimated model.

Such a “reference curve method” has been repeatedly criticized [e.g., *Kamogawa and Kakinami*, 2013; *Masci et al.*, 2015]. In fact, the onset time of the preseismic increase (start of the excluded time interval) has not been constrained in an objective way. STEC always draw U-shaped curves coming from changing elevation angles of satellites, and such curvature often hampers intuitive recognition of the start and the end of subtle anomalies. The reference curve method is essentially impractical for short-term earthquake prediction. Even if we could constrain the onset of the anomalies, we need the TEC data after earthquakes to pin down the reference curves (extrapolation from the preseismic part is hardly satisfactory). After all, unless we explore new methods, we cannot even plot the TEC anomaly map (such as Figure 3 of *Heki* [2011]) before we observe TEC after the occurrence of the earthquake.

2.2. Conversion From STEC to Absolute VTEC

To improve intuitive anomaly recognition, *Heki and Enomoto* [2013] converted STEC to absolute VTEC by importing interfrequency biases (IFB) from external sources. In the least squares estimation using the observation

equation (1), the bias B is highly correlated with the coefficients of polynomials, and it is difficult to estimate realistic absolute VTEC without a priori information on B . In the standard process, we first remove integer ambiguities by adjusting the ionospheric linear combination of the phases to those of pseudoranges. The remaining bias is the sum of the receiver IFB and the satellite IFB. For the Japanese GEONET (GNSS Earth Observation Network) stations, these values are routinely calculated and made available on the Web [Sakai, 2005]. *Heki and Enomoto* [2013] used them and drew absolute VTEC time series. The absolute VTEC showed clear preseismic increases as well as postseismic drops and enabled *Heki and Enomoto* [2013] to demonstrate that the preseismic increases and postseismic decreases are comparable (their Figures 1–3).

In this study, we follow the same procedure to get the absolute VTEC time series before and after eight major earthquakes. The earthquakes include the 2004 Sumatra-Andaman (M_w 9.2), 2011 Tohoku-oki (M_w 9.0), 2010 Maule (M_w 8.8), and 1994 Hokkaido-Toho-Oki (M_w 8.3) earthquakes studied earlier by *Heki* [2011]. We add the 2007 Bengkulu (M_w 8.5) earthquake studied later by *Cahyadi and Heki* [2013], and the main shock (M_w 8.6) and the largest aftershock (M_w 8.2) of the 2012 North Sumatra earthquake, whose coseismic ionospheric disturbances (CID) were studied by *Cahyadi and Heki* [2015]. We also analyzed the TEC before and after the 1 April 2014 Northern Chile (Iquique) earthquake (M_w 8.2) [e.g., *Meng et al.*, 2015]. Satellite IFBs and the receiver IFBs of major IGS (International GNSS Service) stations are available in the header of the global ionospheric model files [Mannucci *et al.*, 1998]. For non-IGS stations, we inferred their receiver IFBs by minimizing the absolute VTEC fluctuations during nighttime following *Rideout and Coster* [2006] (Figure S1 in the supporting information).

Figure 1 shows the absolute VTEC before and after the eight major earthquakes converted from STEC in this way. As shown in *Heki and Enomoto* [2013], the 2011 Tohoku-oki earthquake occurred at 14:46 in local time (LT), and the absolute VTEC was gently decreasing from ~ 30 total electron content units (TECU) to ~ 15 TECU (1 TECU corresponds to 1×10^{16} el m^{-2}) due to the increasing solar zenith angle. The 2010 Maule earthquakes occurred in the middle of the night (03:34 LT). So the absolute VTEC stayed fairly low (< 5 TECU) for hours before and after the earthquakes. The 2004 Sumatra-Andaman occurred in the morning (07:58 LT), when the VTEC was rapidly rising. The 2012 North Sumatra earthquakes, main shock and aftershock, occurred in the afternoon (15:38 LT and 17:43 LT, respectively), and the 2014 Iquique earthquake occurred in the evening (20:46 LT). However, their VTEC showed large irregular changes irrelevant to diurnal variations. In these cases, VTEC shows temporary increase when the line-of-sight vectors cross equatorial ionization anomalies (EIA).

The degree of the polynomial was 2–4 for all cases except the 2014 Iquique event, in which we had to increase it to 9. Another set of data for the eight earthquakes using different pairs of stations and satellites are given in Figure S2. Their geographical details are shown in Figure 2. In both Figures 1 and S2, we could intuitively recognize preseismic VTEC increase and postseismic recovery. There, we drew “reference curves” as we did in *Heki and Enomoto* [2013]. Although it became easier to identify the onset of the anomaly by the STEC to VTEC conversion, we still need the data after earthquakes to draw such reference curves. In the next section, we explore a new method in which we do not rely on reference curves.

2.3. Numerical Method to Detect Positive Breaks

The Akaike’s information criterion (AIC) [Akaike, 1974] is a useful concept to select the optimum model in the least squares estimation. In crustal deformation studies, AIC has been found useful in detecting small but significant discontinuities in coordinate time series caused by slow slip events in SW Japan [Nishimura *et al.*, 2013] and in the Ryukyus [Nishimura, 2014]. We follow *Nishimura et al.* [2013] to detect discontinuous changes in rates (breaks) in the time series. We assume that the TEC measurement errors are uncorrelated and obey the Gaussian distribution with standard deviation σ , and then AIC is calculated (constant terms are removed) as

$$\text{AIC} = n \ln \sigma^2 + 2k, \quad (3)$$

where k is the number of free parameters, n is the number of data, and σ^2 is inferred as the average of the squares of the postfit residuals.

First, we set up a time window and fit the time series within the window in two different ways, i.e., simple linear function ($k=2$) (Case 1), and linear changes with a break at the middle of the window ($k=3$) (Case 2). Always, σ^2 is less in Case 2, but k is larger by 1 in Case 2. We consider Case 2 more appropriate (i.e., the break is significant) if AIC decreased in Case 2. The AIC drop is a measure of significance of the break, and we refer to it as $-\Delta\text{AIC}$.

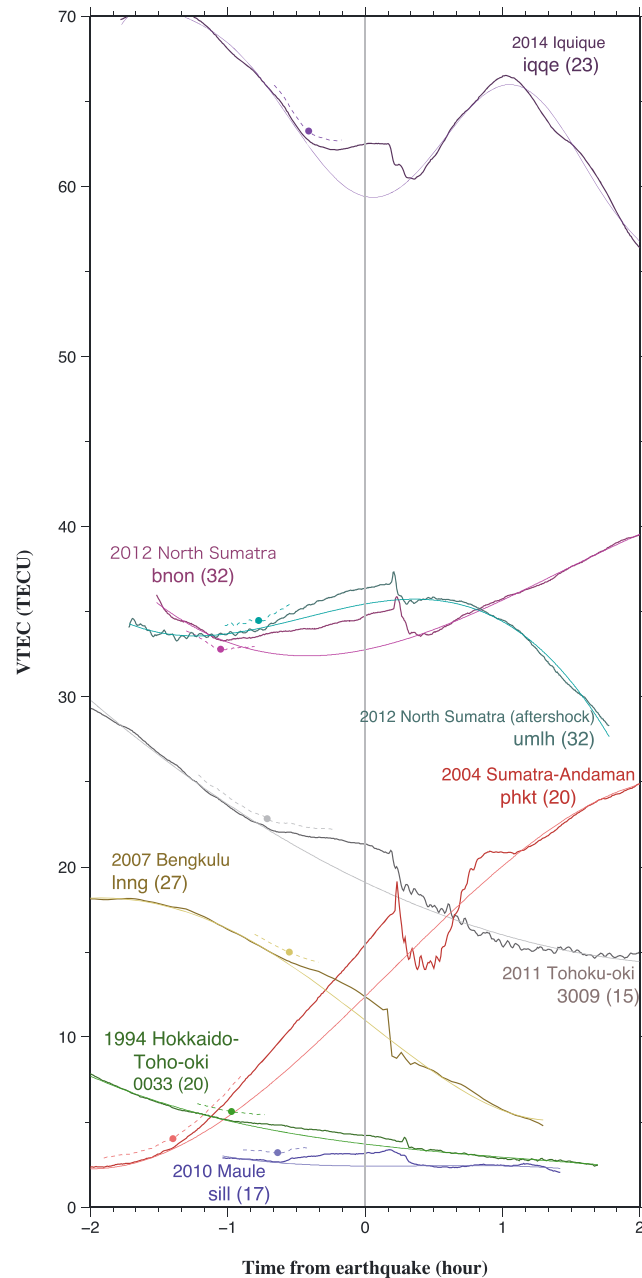


Figure 1. Absolute VTEC time series of ± 2 h around the eight large earthquakes studied here (thick curves). Thin curves are reference curves obtained directly modeling the absolute VTEC using polynomials excluding certain time intervals. The end of the excluded time intervals is $+20$ min of the earthquake, but the start of the excluded time intervals is determined by the peak of $-\Delta AIC$ indicated by solid circles (see text). GNSS station names and GPS satellite numbers are attached to the curves (see Figure 2 for positions). Sizes of the precursors are represented by the change in slope in the middle of the time window of 15–30 min shown by dashed curves. An alternative data set of the eight earthquakes with different satellite-site pairs is shown in Figure S2.

occurrence time, which suggests coherent increase of absolute VTEC after the onset of the precursor without further significant breaks. The amount of break (increase of the rate) shown in colors slightly change in time, depending on the sharpness of the break and the existence of curvature in the absolute VTEC time series

We move the window forward in time and calculate $-\Delta AIC$. Then, we obtain the time series of $-\Delta AIC$, and significant breaks are marked as their peaks. Because we are interested in positive breaks (abrupt increase of the rate), we make $-\Delta AIC = 0$ when the estimated breaks are negative.

In Figures 3a1, 3b1, and 3c1, we plot the $-\Delta AIC$ time series for the three $M9$ class megathrust earthquakes. In each case, we compare results from the two different time windows, i.e., ± 30 min and ± 40 min for the 2011 Tohoku-oki and the 2004 Sumatra-Andaman earthquakes. Considering the shortness of the time series, ± 15 and ± 20 min windows were used for the 2010 Maule earthquake. In all the examples, single significant positive breaks are detected at ~ 40 min (Tohoku-oki and Maule) and ~ 80 min (Sumatra) before earthquakes. Figure 3d shows those for other five earthquakes. There were also single positive breaks found except for the 1994 Hokkaido-Toho-oki earthquakes, before which two comparable breaks were found at ~ 80 and ~ 60 min before the earthquake (we use the latter in comparing properties of the break in the next section).

Figure 3 suggests that a longer time window shows the sharper $-\Delta AIC$ peak and more stable detection of the breaks. However, a ± 40 min window requires a data set spanning 80 min. This means that we can only calculate $-\Delta AIC$ at the epoch ~ 40 min before earthquake just immediately before the earthquake, which is impractical for real-time monitoring. In Figures 3a2, 3b2, and 3c2, we simulate what we can do in real time. There, we first detect significant positive breaks using a relatively short time window (± 10 min in this case). Then, we could fix the center of the window to the detected break and widen the window as the time elapses. In these three cases, the significance ($-\Delta AIC$) steadily increases with time until the earthquake

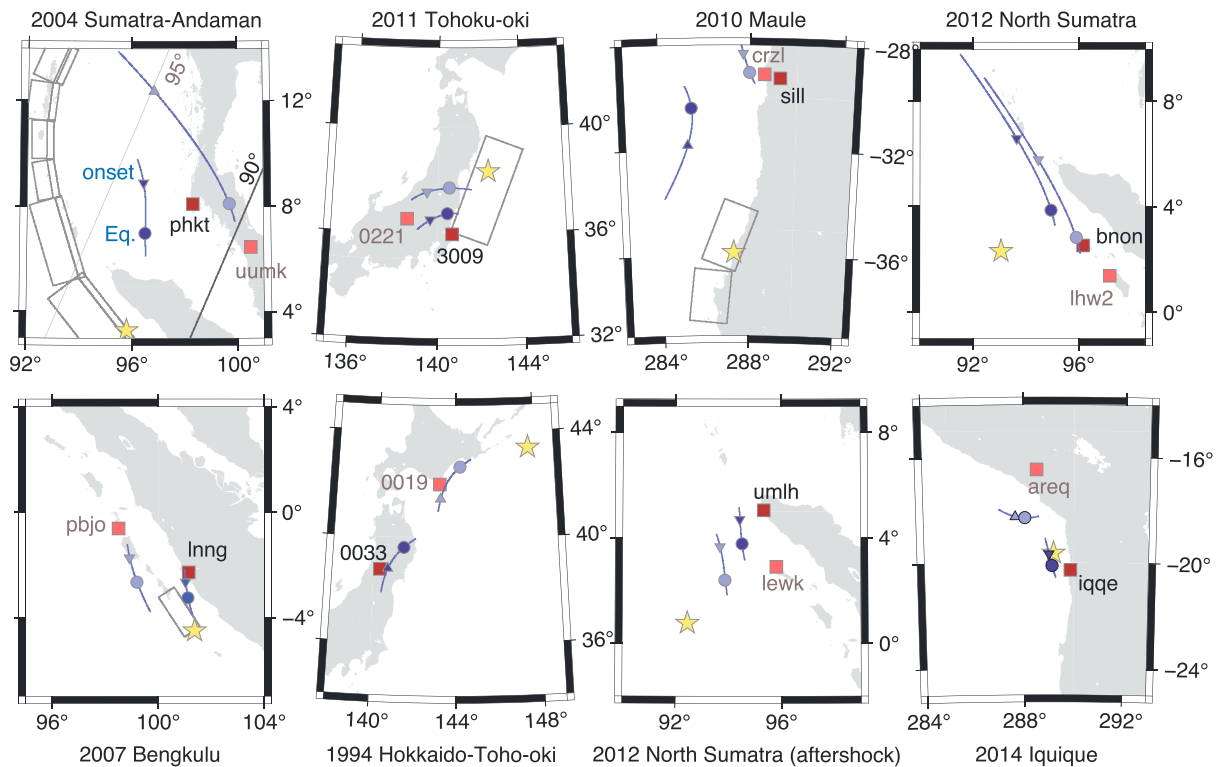


Figure 2. Earthquake epicenters (yellow star) and GNSS stations (red squares) are shown for the eight earthquakes studied here. Subionospheric point (SIP) tracks (blue curves) and SIP positions at the onset of the precursors (blue triangles) and at the time of earthquakes (blue circles) are shown for two sets of data (the darker/brighter color is for those in Figure 1/ Figure S2). SIP was calculated assuming the altitude of the anomaly at 200 km following *Kuo et al.* [2014]. In the 2004 Sumatra-Andaman earthquake, SIPs were located between the two lines corresponding to the solar zenith angles of 90 and 95° when the positive break occurred.

(conversion from STEC to absolute VTEC was necessary to reduce such curvatures). In Figure 1, onsets of the precursory ionospheric electron enhancements are determined in this way as shown with colored circles and dashed curves corresponding to the time window used to detect the breaks. We emphasize that this new method does not need any reference curves or data after earthquakes.

3. Results: Sizes and Times of Precursors and M_w

3.1. Data Analysis of the Eight Earthquakes

Figure 3 shows that significant positive breaks are seen in the time range between 25 min and 80 min before the eight earthquakes studied here. There, we adopted the time window of either ± 30 min (2011 Tohoku-oki and 2004 Sumatra-Andaman) or ± 15 min (all others). In Figure 3d, we set up additional criteria; i.e., $-\Delta AIC$ was made 0 if the rate change is less than the absolute and relative thresholds. The threshold was 1 TECU/h (absolute) and 25% (relative).

Heki [2011], in its Figure 4b, compared sizes of the precursors of four earthquakes as the cumulative departure of the data from the reference curves at their occurrence times. This quantity, however, depends on the definition of reference curves. Here we define the size of the precursor as the increase of the VTEC rate (difference between the VTEC rates between the left and right halves of the time window; see Figure 3a1) when the significant break is detected by $-\Delta AIC$. In Figure 4a, we compare such sizes of breaks inferred in this way. These quantities do not depend on the definition of the reference curves in any sense. We use $-\Delta AIC$ just to detect breaks and do not use them in comparing the precursors of different earthquakes. By the way, the reference curves in Figures 1 and S2 were drawn using the onset times of the precursors (starts of the excluded time intervals) objectively determined here (the end of the excluded time interval is fixed to 20 min after earthquakes, except the 2004 Sumatra-Andaman case in Figure S2).

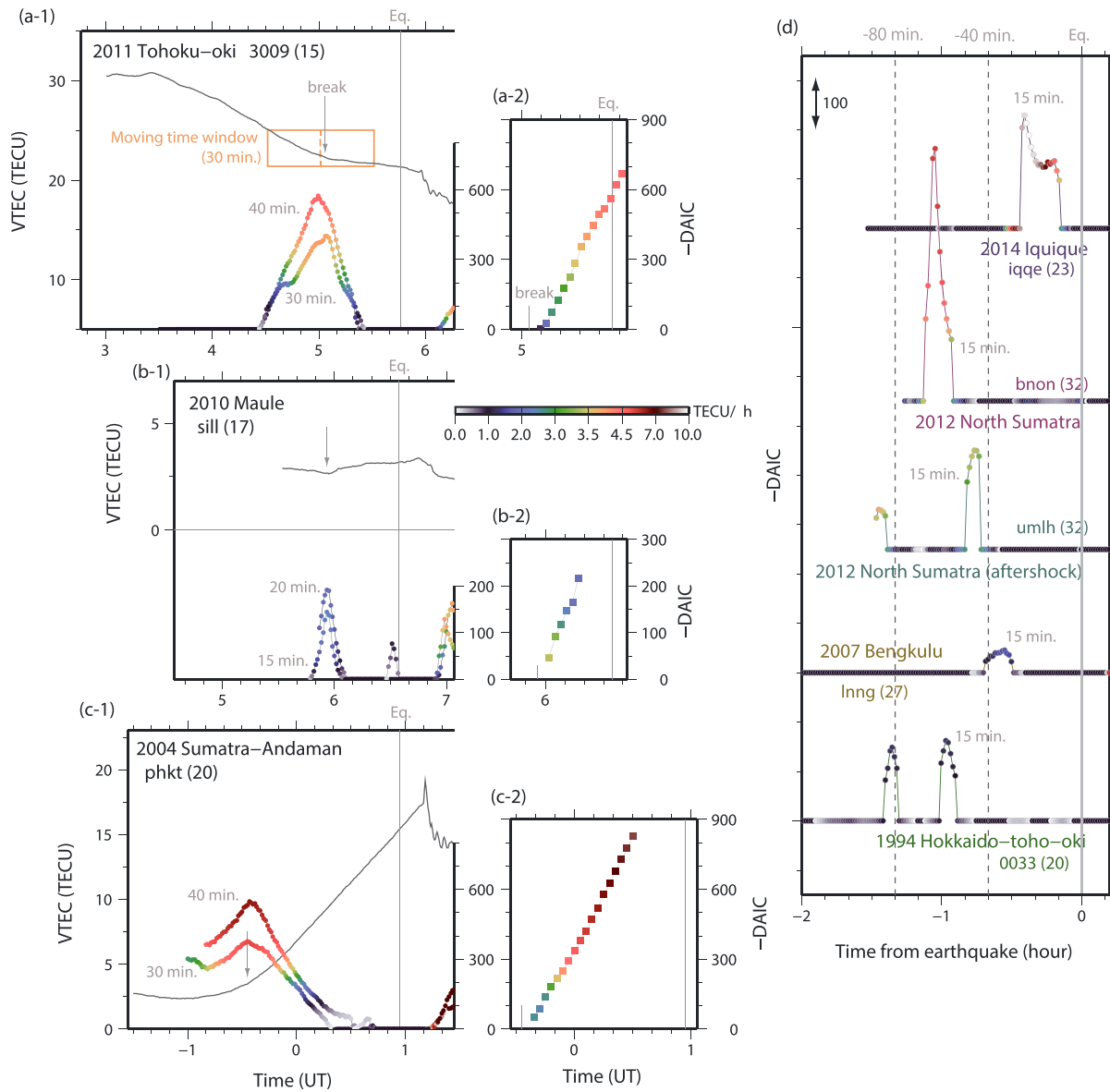


Figure 3. Absolute VTEC curves before the (a1) 2011 Tohoku-oki, (b1) 2010 Maule, and (c1) 2004 Sumatra-Andaman earthquakes, and the behavior of $-\Delta AIC$ (significance of the break) are shown with colored circles. A brown rectangle in Figure 3a shows an example of a moving time window to calculate $-\Delta AIC$. The color represents the detected amount of breaks (abrupt changes in slope). Two different time windows are used for calculating $-\Delta AIC$. (a2, b2, and c2) The increase of the significance as we expand the time windows fixing the center of the window at the detected break. (d) Similar plot of $-\Delta AIC$ for the other five earthquakes are also given, where time windows were all 15 min. We picked up breaks larger than 3.0 TECU/h and 75% of the original slopes. This threshold was lowered to 1.0 TECU/h and 20 % for the 1994 and 2007 earthquakes. The 1994 Hokkaido-Toho-oki earthquake has a secondary peak ~ 20 min earlier than the largest peak. Other earthquakes show single clear peaks before the earthquakes.

The 2011 Tohoku-oki earthquake showed the break of ~ 3.9 TECU/h. This is consistent with the cumulative anomaly of ~ 2.5 TECU as shown in Figure 4b of *Heki* [2011] because the enhanced rate lasted ~ 40 min. The largest precursor, ~ 10 TECU/h, is seen before the 2014 Iquique earthquake. The break before the 2010 Maule earthquake is slightly larger than 2 TECU/h in spite of its seismic moment being nearly an order of magnitude larger than the 2014 Iquique event. Obviously, the breaks are not simply bigger for larger earthquakes. This will be discussed in the next section.

The onset times of the eight earthquakes also showed variety (Figure 5a). The onset of the precursors of the four earthquakes, 2011 Tohoku, 2010 Maule, 2007 Bengkulu, and the aftershock of the 2012 North Sumatra earthquakes concentrate around 40 min before the earthquakes (although *Masci et al.* [2015] considered it

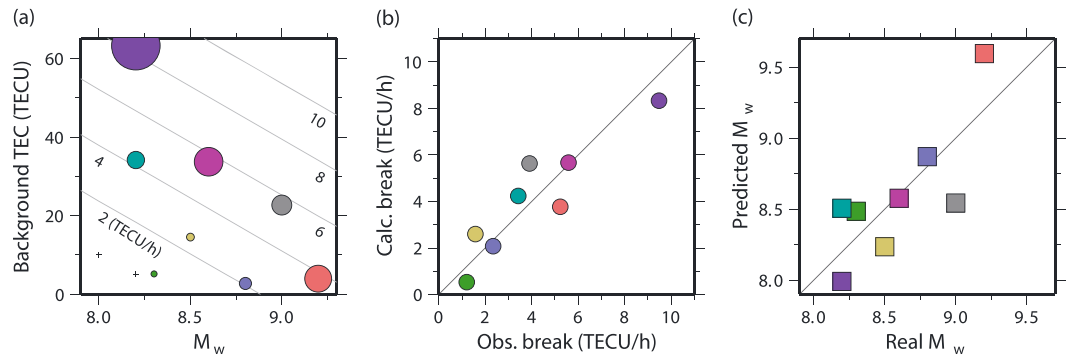


Figure 4. (a) The amount of the breaks (expressed as the size of the circles) are plotted as functions of the two factors, i.e., the M_w of the earthquakes (horizontal axis) and the background absolute VTEC (vertical axis). The observed breaks are 3.91 (Tohoku, gray), 2.34 (Maule, blue), 5.24 (Sumatra-Andaman, red), 1.21 (Hokkaido-Toho-oki, green), 1.59 (Bengkulu, yellow), 5.58 (North Sumatra main shock, purple), 3.43 (North Sumatra aftershock, blue-green), and 9.48 (Iquique, deep purple) TECU/h. The break is modeled as $3.78 M_w + 0.14 \text{ VTEC} - 31.6$, and the contour lines (based on this model) showing the same break size are shown for 2, 4, 6, 8, and 10 TECU/h. (b) We compare the observed break with those calculated with the above model using absolute VTEC and M_w as inputs. The RMS of the scatter is ~ 1.04 TECU/h. (c) We compare the real M_w of the eight earthquakes and those predicted using the observed break size and the background absolute VTEC using equation (5). The RMS of the difference in M_w between the two is ~ 0.28 . Colors of the symbols for different earthquakes are adopted from Figure 1.

unnatural and wrong). However, the precursor of the largest (2004 Sumatra-Andaman earthquake, $M_w 9.2$) and the smallest (2014 Iquique earthquake, $M_w 8.2$) earthquakes started ~ 80 min and ~ 25 min before earthquakes, respectively. Hence, Criticism #3 of Masci *et al.* [2015] is about something we did not claim (earlier start of the TEC anomaly before the 2004 Sumatra-Andaman earthquake is already reported in the first paper [Heki, 2011]).

3.2. Sizes of the Precursors

One may find it strange that the 2014 Iquique earthquake showed the largest break of all (~ 10 TECU/h). In Figure 1, one can notice that this earthquake occurred under the largest background absolute VTEC (> 60 TECU) because of the penetration of line of sight with EIA. In Figure 4a, large breaks are shown with large circles, and we took earthquake M_w and the background TEC as the horizontal and the vertical axes, respectively. The figure suggests that the breaks tend to be larger before large earthquakes and under higher background absolute VTEC. Here we hypothesize that the break is a function of both M_w and the background absolute VTEC.

It seems natural that a larger earthquake is preceded by a larger precursor. The absolute VTEC dependence is understandable if the precursors are made by electron transportations within ionosphere as suggested by Kuo *et al.* [2014]. Larger electron density would be needed to redistribute more electrons. We assume an empirical model in which the break, $\Delta(d\text{VTEC}(t)/dt)$, is linearly dependent on M_w and background absolute VTEC, i.e.,

$$\Delta(d\text{VTEC}(t)/dt) = A M_w + B \text{ VTEC} + C. \tag{4}$$

The least squares estimation, with equation (4) as the observation equation, revealed that the combination of $A = 3.78$, $B = 0.14$, and $C = -31.6$ best reproduces the breaks before the eight earthquakes. Figure S4 shows that geomagnetic activity indices at the occurrence times of the eight earthquakes are not correlated with such breaks. In Figure 4b, we compare the observed and calculated breaks, and the root-mean-squares of their differences were 1.04 TECU/h. The 2004 Sumatra-Andaman earthquake shows the largest departure of the observed and calculated break. That positive break of VTEC before this earthquake might have been intensified by the natural increase caused by the sunrise, nearly coincident with the onset of the precursor (at that time, subionospheric points (SIPs) are located between lines of solar zenith angles of 90 and 95°; see Figure 2).

Figure 4a includes contour lines for the predicted breaks of 2, 4, 6, 8, and 10 TECU/h. We can see that the precursors are visible for $M9$ class earthquakes even when the background is no more than a few TECU.

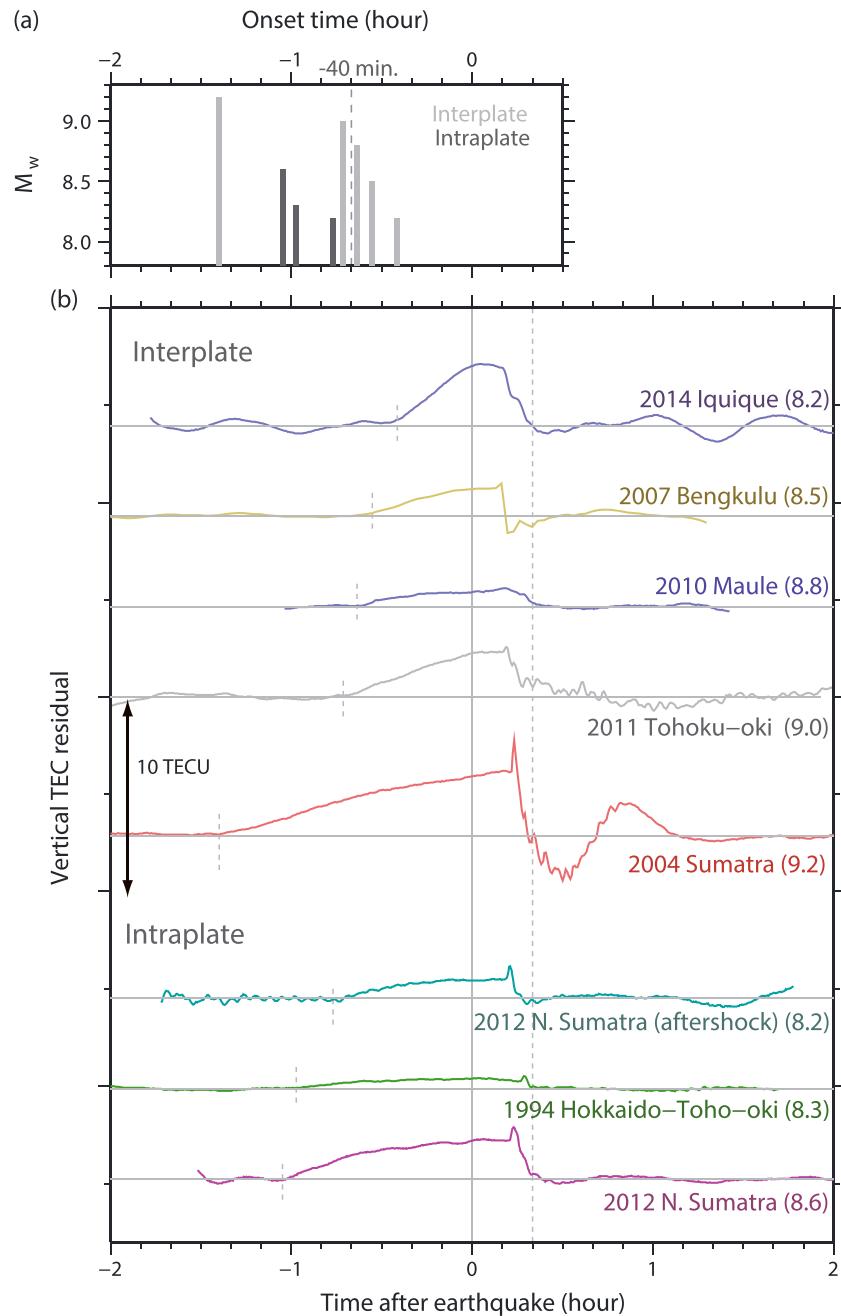


Figure 5. (a) Comparison of the onset times of the precursory TEC enhancement for earthquakes with various M_w . Precursors tend to start earlier before larger earthquakes and intraplate earthquakes (dark gray). (b) The residual plot of VTEC for the eight earthquakes are compared. M_w is indicated within the parentheses. Short vertical dashed lines indicate the times of positive breaks. For the site name and satellite numbers, see Figure 1.

On the other hand, $M_{8.5}$ class earthquakes need to occur under absolute VTEC of ~ 10 TECU or more to make a break as strong as ~ 2 TECU/h (possibly the level to be detected real time). We can lower the M_w to 8.2 if the background absolute VTEC is higher than 20 TECU. Figure 4a also includes two earthquakes for which *Heki* [2011] failed to find TEC precursors, i.e., the 2003 Tokachi-oki ($M_w 8.0$) and 2007 central Kuril earthquakes ($M_w 8.2$). Obviously, M_w and background absolute VTEC of these two events are not large enough to warrant recognizable precursory breaks. In Figure S2, we give an alternative set of absolute VTEC data for the eight earthquakes. The basic picture remains the same for this data set.

Equation (4) can be modified as

$$M_w = \{\Delta(\text{dVTEC}(t)/\text{dt}) - B \text{ VTEC} - C\}/A. \quad (5)$$

This equation would let us infer M_w of the impending earthquake with 1 sigma uncertainty of ~ 0.28 by measuring the precursory VTEC break and the background absolute VTEC in real time (Figure 4c). Overestimation of M_w for the 2004 Sumatra-Andaman would be due to the excessive positive break due to the sunrise. The accuracy of the coefficients A–C would be improved as relevant data accumulate in the future, which is important to make the TEC monitoring useful for short-term earthquake prediction someday.

3.3. Onset Times of the Precursors

Figure 5a compares the start times of the precursors of the eight earthquakes. They range from ~ 25 min (2014 Iquique, $M_w 8.2$) to ~ 80 min (2004 Sumatra-Andaman, $M_w 9.2$) before the earthquakes. We expect that a larger earthquake may have a longer precursor time. However, the observed relationship is a little more complicated. For example, the precursor of the $M_w 8.6$ North Sumatra earthquake occurred more than an hour before the main shock, significantly earlier than ~ 40 min for the $M_w 9.0$ Tohoku-oki earthquake.

The relationship would become natural if we divide the earthquakes into intraplate (dark gray in Figure 5a) and interplate (light gray in Figure 5a) earthquakes. The intraplate earthquakes are the 1994 Hokkaido-Toho-Oki earthquake and the 2012 North Sumatra main shock and its largest aftershock. The former may have torn the Pacific Plate slab [e.g., *Tanioka et al.*, 1995], and the latter occurred as strike-slip events to the west of the Sunda Trench within the subducting oceanic plate [e.g., *Meng et al.*, 2012]. The other five earthquakes are all interplate megathrust events. Within the two groups, precursors tend to occur earlier before larger earthquakes (Figure 5a).

For future practical short-term earthquake prediction, it may be difficult to tell whether the impending earthquake is an interplate megathrust or a slab earthquake. In either case, the earthquakes are anticipated to occur in a range from 25 to 80 min depending on M_w inferred from the observed break and equation (5). By the way, the 1994 Hokkaido-Toho-oki earthquake showed two comparable breaks at ~ 80 and ~ 60 min before the earthquake (Figure 3d). Another example in Figure S2, closer to the epicenter, showed only one break at ~ 80 min before the earthquake, a precursor time comparable to the $M_w 9.2$ 2004 Sumatra-Andaman earthquake.

A major difference between intraplate and interplate earthquakes would be the stress drop; i.e., the former have stress drops twice as large as the latter on average [*Kato*, 2009; *Allmann and Shearer*, 2009]. The mechanisms of precursory TEC increases are little known, but it might be a process that would take more time before earthquakes with higher stress drops. Anyway, we could cancel the warnings for impending earthquakes confidently if the earthquake does not occur within 1.5 h after detecting significant positive breaks.

4. Discussions

4.1. TEC Breaks and Space Weather

We showed that large earthquakes are preceded by sudden increases of VTEC rate 25–80 min before earthquakes. In fact, there are no recent earthquakes with M_w of 8.5 or more without such signatures (excluding the 2005 Nias earthquake, $M_w 8.6$, for which plasma bubbles hampered the detection [*Cahyadi and Heki*, 2013]). *Heki and Enomoto* [2013] suggested that large-scale traveling ionospheric disturbances (LSTIDs) often make signatures similar to preseismic anomalies. Now we examine how often such positive breaks occur during times of no earthquakes due to space weather. If they occur every hour, all the breaks found before earthquakes (Figure 1) would be fortuitous. However, if they occur only once in a day, the probability of their occurrences would be too small to be fortuitous.

Figures 6a–6c are adopted from Figures 6b–6d of *Heki and Enomoto* [2013]. There we show 4 h absolute VTEC curves from GPS satellite 15 and station 3009 over 3 weeks. The geomagnetic activity was low during the first week and high during the second and the third weeks (*AE*, *Dst*, and *Kp* indices are shown in Figure 6a of *Heki and Enomoto* [2013]). We performed the same $-\Delta\text{AIC}$ analysis as in Figure 3. There we selected only breaks larger than prescribed absolute (>3.0 TECU/h) and relative ($>75\%$ of the original rate) thresholds.

We detected seven such breaks (labeled with numbers 1–7) including the one that occurred ~ 40 min before the Tohoku-oki earthquake (~ 3.9 TECU/h). Their signatures are similar to preseismic VTEC breaks (Figure S5a).

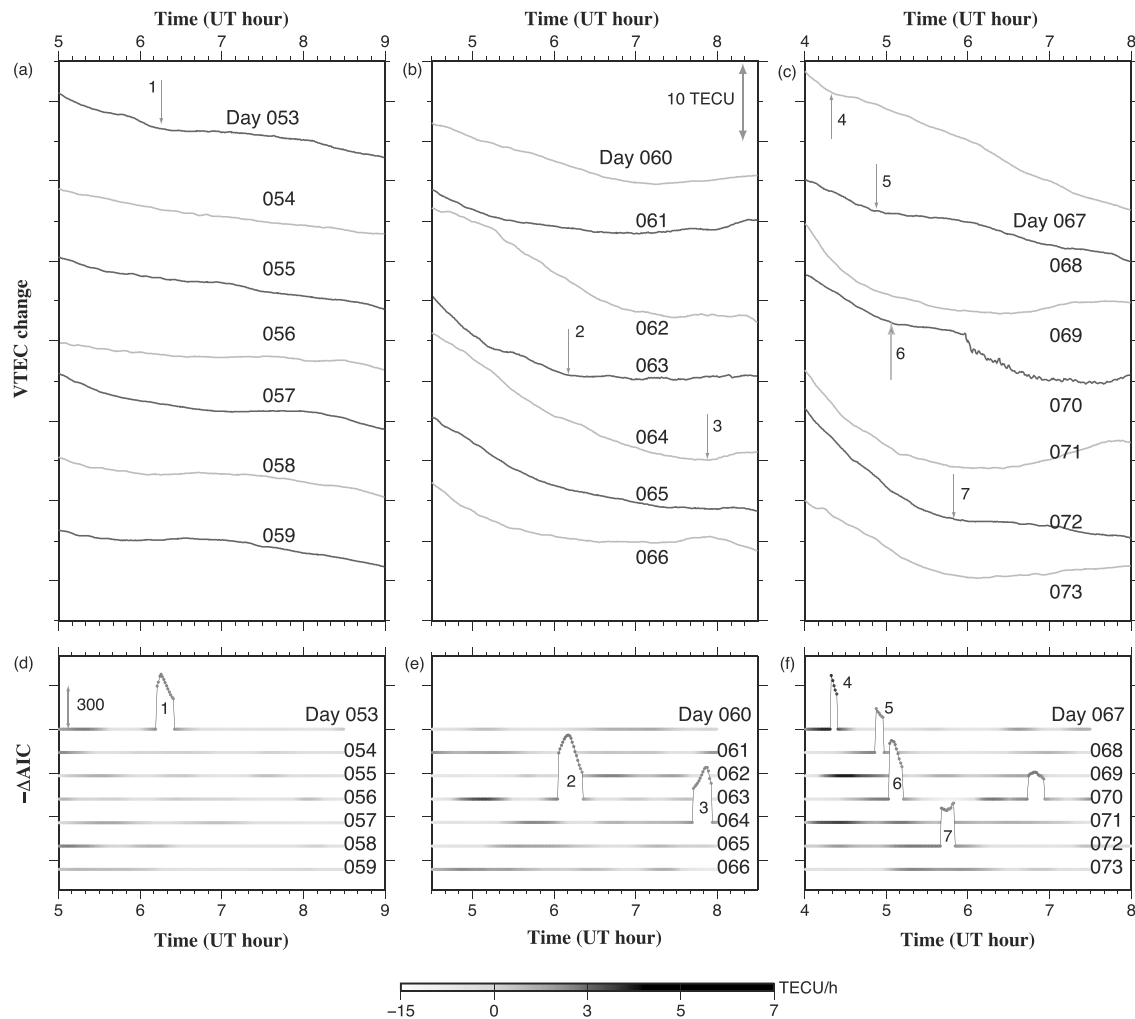


Figure 6. (a–c) VTEC time series for the 3 week period (same data set as in *Heki and Enomoto* [2013]) of the same pair of the satellite (GPS 15) and station (3009). The geomagnetic activity was calm in the first week and severe in the second and third weeks. (d–f) By calculating $-\Delta AIC$ (time window is ± 30 min), we could detect six significant positive breaks, larger than 3 TECU/h and 75% of the original rate, in addition to the preseismic one on day 070 (they are numbered as 1–7). These breaks propagate southward (Figure 7) and are considered to be parts of small-amplitude LSTIDs.

Hence, the average rate of occurrence of breaks exceeding 3 TECU/h in 1 h is below 0.1. This probability is highly dependent on the threshold (Figure S5b). In Figure S6, we show the 5 h absolute VTEC curves of the same site-satellite pair over a 4 month period. There significant positive breaks (exceeding 3.5 TECU/h) are detected 31 times. Then, the average hourly occurrence rate of such breaks is $\sim 1/20$.

We did not perform such long-period analyses for other localities (e.g., Indonesia and Chile), but this probability would be less considering high geomagnetic activities before and after the 2011 Tohoku-oki earthquake (Figure S4) and higher LSTID occurrence rates in spring and autumn [*Tsugawa et al.*, 2004]. Figure 4b shows that five earthquakes are preceded by positive breaks larger than 3 TECU/h. If such breaks randomly occurred with a probability of 1/10 per hour, the detection probability of such breaks over 1.5 h periods before these earthquakes would be $(1.5 \times 1/10)^5$. This is small enough to let us rule out the fortuity of these breaks. Figures 6 and S6 suggest that the detected breaks concentrate on the week of the high geomagnetic activity.

Heki and Enomoto [2013], in their Figure S4, showed that the breaks on days 068 and 072 propagate southward with the velocity suggesting their internal gravity wave origin. This indicates that these breaks are parts of small-amplitude LSTIDs related to auroral activities. By the way, the break at $\sim 05:00$ UT on day 068 was mentioned in *Masci et al.* [2015] as an example showing enhancement without a notable earthquake 40 min later, although they did not quote our analysis shown in Figure S4 of *Heki and Enomoto* [2013].

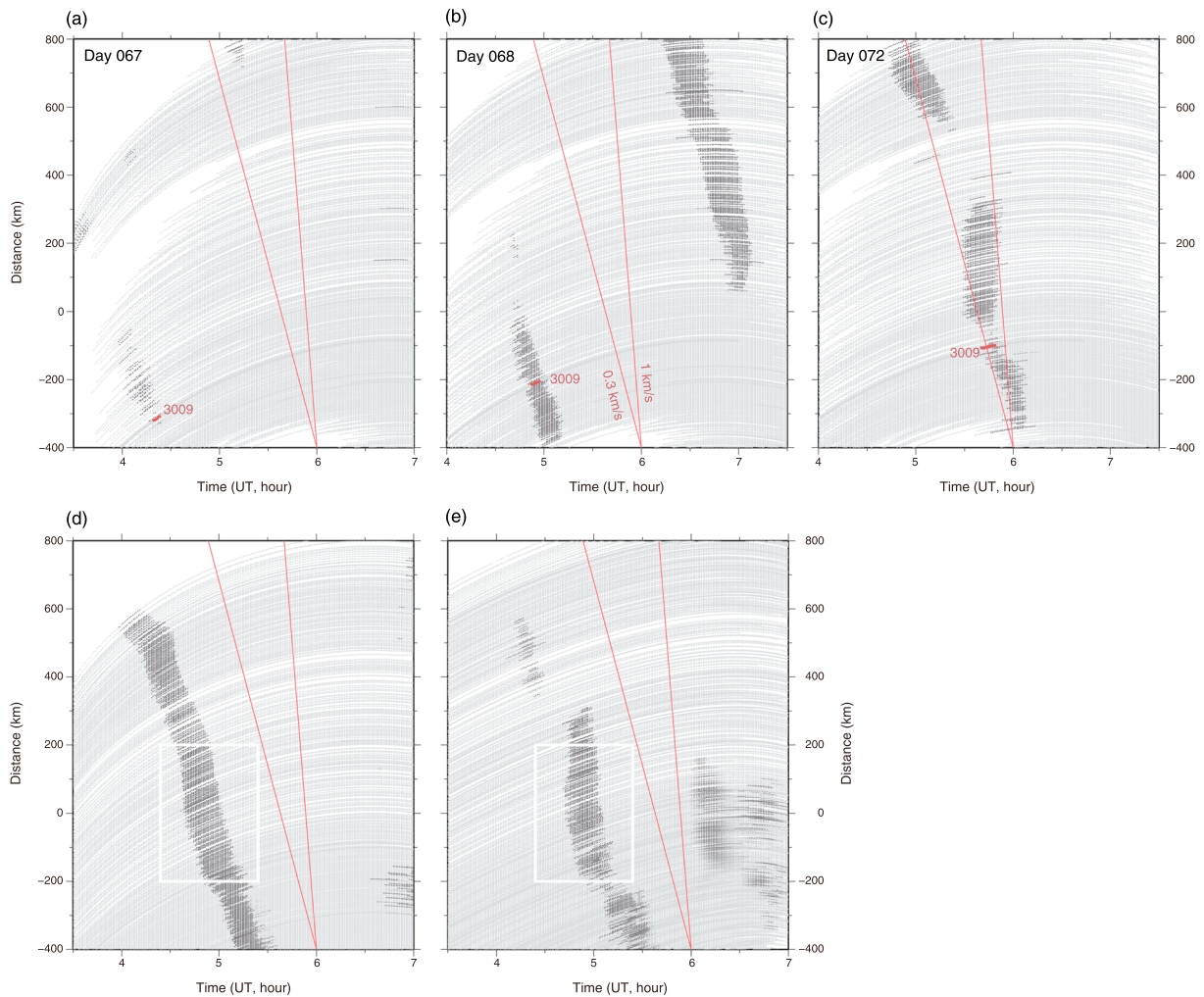


Figure 7. For the three cases of the detection of significant positive breaks on the days of no earthquakes, (a) days 067, (b) 068, and (c) 072, corresponding to anomalies #4, #5, and #7 in Figure 6c, we plot $-\Delta\text{AIC}$ as shown in Figure 6f for all available stations as the functions of UT (horizontal axis) and the distance along NE Japan. The origin is taken at 140°E , 38°N , and the distance is measured in the direction $\text{N}15^\circ\text{E}$. One line corresponds to the plot of $-\Delta\text{AIC}$ observed at one of the ~ 1200 GEONET stations. The detections of significant positive breaks are indicated with black. In all the three cases, occurrence of the breaks gets later as we go southward, suggesting that they are LSTID propagating from the auroral region. For the $-\Delta\text{AIC}$ time series at station 3009, shown in Figure 6f, the break detections are marked with red. Below we show similar plots for the earthquake day (day 070) with (d) Satellites 15 and (e) 26. White rectangles show approximate extent of the fault of the 2011 Tohoku-oki earthquake.

In a statistical study of many LSTIDs in Japan, *Tsugawa et al.* [2004] showed that their average propagation was southward with the speeds $0.3\text{--}0.6\text{ km/s}$. They found that LSTID occurrence rate is highly dependent on geomagnetic activities in high latitudes and $\sim 3/4$ LSTIDs occur during periods of $Kp \geq 4$. Here we study the cases on the days 067, 068, and 072, labeled as the anomalies 4, 5, and 7 in Figures 6c and 6f, using the new method utilizing $-\Delta\text{AIC}$, with the absolute VTEC time series not only at site 3009 but at all the GEONET stations in Japan. In Figures 7a–7c, we marked detected positive $-\Delta\text{AIC}$ with dark color as the function of time and geographical position of subionospheric point (SIP). It is clearly shown that the breaks tend to occur at later times as we go farther southward along NE Japan. This confirms our results in *Heki and Enomoto* [2013] that they are parts of LSTID propagating from the auroral region to midlatitude. The overall velocity is $\sim 0.3\text{ km/s}$, suggesting their internal gravity wave origin.

We show similar plots for the day of the earthquake (day 070) in Figures 7d and 7e using GPS satellites 15 and 26, respectively. As reported earlier [*Heki and Enomoto*, 2013, Figure 7a], Satellite 15 clearly recorded a small but clear LSTID propagating southward through NE Japan, and this is clear in the plot of Figure 7d. After all, it may not be easy to distinguish, only by seeing these diagrams, positive breaks due to the earthquake (Figures 7d and 7e) from those due to space weather (Figures 7a–7c). The appearances of the breaks within

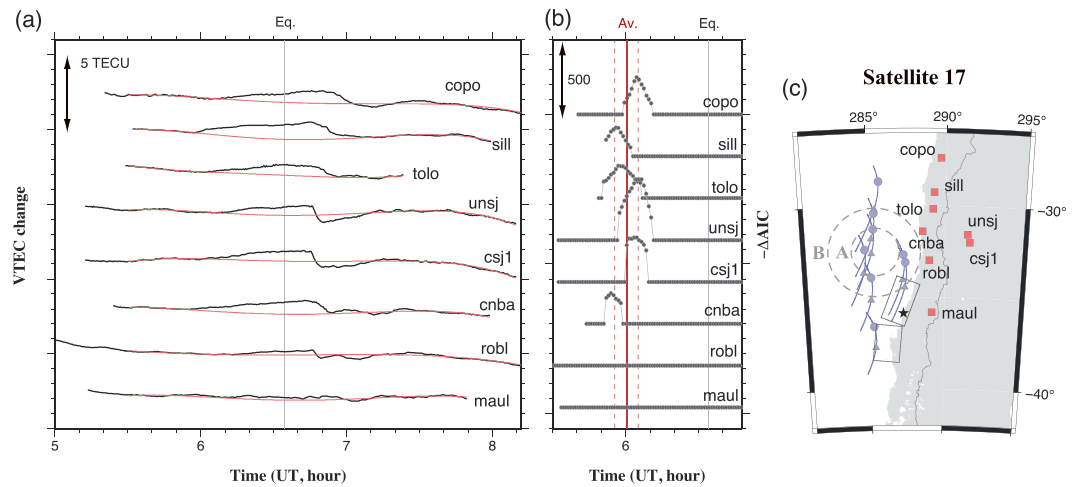


Figure 8. (a) Absolute VTEC time series before and after the 2010 Maule earthquake (M_w 8.8) at eight stations in Chile and Argentina observed with GPS satellite 17. Precursory VTEC increases are clear at SIPs to the north of the epicenter (within circle B) and are absent outside. (b) We compare $-\Delta AIC$ behaviors of the curves in Figure 8a (thresholds are 1.1 TECU/h and 50%, and the time window is ± 20 min). (c) SIP tracks are drawn assuming 200 km as the ionospheric penetration height. The blue triangles and circles show SIP positions at the onset of the precursor (at sill) and at the time of earthquake occurrence, respectively. The $-\Delta AIC$ peaks at the top six stations occurred at 6.01 ± 0.08 UT (vertical red line). Anomalies seem to have started earlier within circle A.

the latitude range of the ruptured fault (white rectangles in Figures 7d and 7e) look more or less simultaneous (especially with Satellite 26), which suggests a certain difference from the signatures of the breaks of space weather origin.

As for the waveforms, the VTEC changes due to LSTID (Figure S5a) look similar to preseismic anomalies and cannot be easily distinguished. We will need a sophisticated system to discriminate the two (this may include a decision to give up discrimination under high geomagnetic activities) and to monitor space weather especially the auroral activities in high-latitude regions which often bring LSTID in midlatitude with the time lag of a few hours.

4.2. Spatial Distribution and Waveforms

Shinagawa *et al.* [2013] numerically simulated the TEC drop that occurred ~ 10 min after the 2011 Tohoku-oki earthquake when acoustic waves from the uplifted surface arrived at the *F* region of the ionosphere. This is essentially a mechanical process to transport electrons outward from the region above the uplifted surface. Although the physical process of preseismic electron enhancements is poorly known, it will possibly be an electromagnetic process involving the lithosphere, atmosphere, and ionosphere as shown in Kuo *et al.* [2014]. The absolute VTEC time series shown in Figures 1 and S2 suggest that such increases and decreases are balanced in a long run, and this is natural considering that both the preseismic and postseismic processes work only temporarily.

According to Kuo *et al.* [2014], upward vertical electric currents in the lithosphere cause lowering of electrons resulting in enrichment and depletion of electrons at heights of 200–250 km and 300–500 km, respectively. Horizontal positions of such anomalies are shifted southward and northward by 100–200 km from the epicenters in the Northern and the Southern Hemispheres, respectively (see their Figure 12). The distributions of the satellite-station pairs that exhibited the largest preseismic signals shown in Figure 2 support this; i.e., largest preseismic signatures tend to be at the southern/northern sides of the rupture area in earthquakes in Northern/Southern Hemispheres. On the other hand, distribution of postseismic electron depletion will occur just above the coseismic surface uplift region [Shinagawa *et al.*, 2013].

Figure 8 shows the absolute VTEC curves from eight GNSS stations around the epicenter of the 2010 Maule earthquake. Relatively large VTEC breaks are seen at six stations, i.e., sill, tolo, cnba, copo, unsj, and csj1, whose SIPs are located 100–200 km to the north of the ruptured fault. On the other hand, little breaks are seen at the two more southerly stations, robl and maul. Figure 8 also suggests some differences in the onset times of the

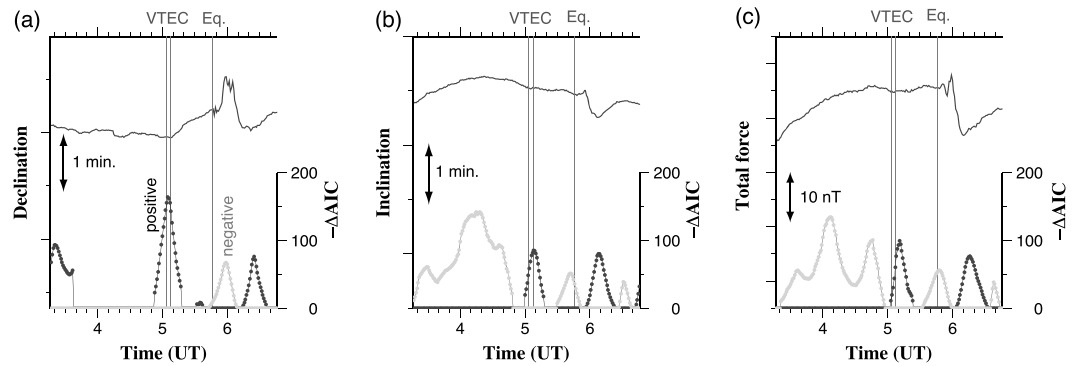


Figure 9. We searched for significant positive breaks in the three components of the geomagnetic field, (a) declination, (b) inclination, and (c) the total force, at the Kakioka station, Kanto, with reference to the Kanoya station, Kyushu (see *Heki and Enomoto* [2013] for their positions), using the same method as in Figure 3. Because we are interested in both increases and decreases, we show $-\Delta\text{AIC}$ plots of not only positive breaks (dark gray) but also negative breaks (light gray). Time windows are set to ± 30 min, and $-\Delta\text{AIC}$ was plotted only for breaks larger than 0.5 (min/h), 0.15 (min/h), and 1.5 (nT/h) for Figures 9a–9c, respectively. We detected significant breaks (all positive) in all the components at time close to the onset of the VTEC anomaly (two lines correspond to those of the VTEC anomaly onset times in Figures 1 and S2).

preseismic TEC enhancements. It started ~ 38 min before the main shock above the SIPs of sill, tolo, and cnba (within circle A of Figure 8c). Then, the enhancement propagated to circle B (Figure 8c), and the stations, copo, unsj, and csj1, with SIPs close to circle B, showed positive breaks at ~ 30 min before the event.

Because physical processes and spatial distribution are different between the preseismic and postseismic processes, temporary imbalance is anticipated to occur. In Figure 5b, although the increasing phases (preseismic process) are more or less similar, waveforms after earthquakes have large variety. For example, the 2010 Maule earthquake shows only gradual decrease after earthquake, but 2014 Sumatra-Andaman earthquake shows excessive initial decrease, and a long-period damped oscillation follows. Such variety is also seen in Figure S3b. These differences would be explained by the shortage and overshoot of the coseismic drops simulated by *Shinagawa et al.* [2013]. In Figure 8, we show that even the same earthquake (2010 Maule) presents different types of waveforms. In the four stations (copo, sill, tolo, and cnba) with SIPs relatively far from the fault, preseismic enhancement is larger than postseismic drop, and recovery occurs slowly. On the other hand, the two stations with SIPs closer to the rupture area (unsj and csj1) show overshoot of postseismic drop and gradual increase after that.

4.3. Geomagnetism

As the last topic in the discussion, we answer Criticism #4 by *Masci et al.* [2015] that they cannot accept the situation that geomagnetic field changes synchronous to the preseismic VTEC changes are seen only in the declination. Figure 9 shows that this is simply not the case. There we plot the declination, inclination, and the total force of the geomagnetic field at Kakioka, Kanto. Following *Utada et al.* [2011], we calculated the difference from the data taken at Kanoya, Kyushu.

It is true that only declination showed the “clear” changes with the reference curve method (Figure 9a). However, if we use the new method using $-\Delta\text{AIC}$ plot, we can see that significant breaks ~ 40 min before the earthquake are seen not only in declination but also in the inclination and the total force (Figures 9b and 9c). Because we do not have a decisive model for the preseismic processes, we do not know in which direction the precursory changes should appear (both positive and negative breaks are shown in Figure 9). Nevertheless, it is clear that *Masci et al.* [2015] criticized what *Heki and Enomoto* [2013] did not claim.

5. Concluding Remarks

In this paper, we answered Criticisms #1–4 in *Masci et al.* [2015], in which Criticism #3 (40 min problem) and Criticism #4 (declination problem) were just based on their misunderstandings. We responded to Criticism #1 (reference curve problem) by proposing a new method without using reference curves. We did not simply rebut to Criticism #2 (natural variability problem). As addressed in *Heki and Enomoto* [2013], the existence of coseismic ionospheric disturbances (CID) is not questioned although their amplitudes are much smaller

than natural variability (for example, sporadic *E* signatures are very similar to CID in amplitudes and periods; see Maeda and Heki [2014, 2015]). That is because they have clear correlation in time and space with the earthquake occurrences.

Here we tried to demonstrate the same; i.e., we explored for temporal and spatial correlation between pre-seismic VTEC change signatures with earthquake properties, e.g., M_w and types, using the eight large earthquakes of M_w 8.2–9.2. We also quantified the probability of the occurrence of nonseismic VTEC breaks similar to those found before earthquakes. We found that those as large as the precursor of the 2011 Tohoku-oki earthquake occur less than once in arbitrary 10 h. Given this probability, we can rule out the possibility that the precursory VTEC changes are just a product of chance.

After all, the findings in this study could be summarized as follows:

1. Preseismic ionospheric enhancement can be detected as positive breaks of VTEC without defining reference curves.
2. Amount of breaks obeys a simple linear relationship with background absolute VTEC and M_w .
3. Breaks occur earlier for larger earthquakes, and those before intraplate earthquakes might occur significantly earlier.
4. Similar breaks could occur by geomagnetic activities, but they are not frequent enough to account for preseismic breaks.

An M_w 7.8 earthquake occurred in Nepal on 25 April 2015, 4 days after the submission of the first version of this paper. Although its magnitude is out of the range of the target earthquakes of our study, observable positive breaks might emerge owing to the large background absolute VTEC (>50 TECU in this case). Heki [2015], using the VTEC data derived at IGS station lck4 in northern India with GPS satellite 26, found that a positive break of ~3.1 TECU/h occurred ~21 min before the main shock. The size is roughly consistent with equation (4), and the occurrence time is consistent with the overall trend shown in Figure 5a. This new example would reinforce the findings given in this paper.

Acknowledgments

We thank F. Masci and his coauthors for motivating us to revisit the preseismic ionospheric electron enhancement. We also thank E. Calais and the other two referees for constructive reviews. We thank C. Vigny (ENS) for private GNSS data in Malaysia and Chile of his group. GNSS data in Japan are available from www.terras.gsi.go.jp upon request. Indonesian GNSS data are available from the SUGAR network website. Geomagnetic data were downloaded from the Japan Meteorological Agency website. This study was partially funded by Kakenhi (26400442).

Alan Rodger thanks Tong Xu, Eric Calais, and another reviewer for their assistance in evaluating this paper.

References

- Akaike, H. (1974), A new look at the statistical model identification, *IEEE Trans. Autom. Control*, *19*, 716–723, doi:10.1109/TAC.1974.1100705.
- Allmann, B. P., and P. M. Shearer (2009), Global variations of stress drop for moderate to large earthquakes, *J. Geophys. Res.*, *114*, B01310, doi:10.1029/2008JB005821.
- Cahyadi, M. N., and K. Heki (2013), Ionospheric disturbances of the 2007 Bengkulu and the 2005 Nias earthquakes, Sumatra, observed with a regional GPS network, *J. Geophys. Res. Space Physics*, *118*, 1–11, doi:10.1002/jgra.50208.
- Cahyadi, M. N., and K. Heki (2015), Coseismic ionospheric disturbance of the large strike-slip earthquakes in North Sumatra in 2012: M_w dependence of the disturbance amplitudes, *Geophys. J. Int.*, *200*, 116–129.
- Heki, K. (2011), Ionospheric electron enhancement preceding the 2011 Tohoku-Oki earthquake, *Geophys. Res. Lett.*, *38*, L17312, doi:10.1029/2011GL047908.
- Heki, K. (2015), Ionospheric electron enhancement ~20 minutes before the 2015 Nepal earthquake, paper presented at the 2015 Gen. Assembly Jap. Geosci. Union, Chiba, 25 May.
- Heki, K., and Y. Enomoto (2013), Preseismic ionospheric electron enhancements revisited, *J. Geophys. Res. Space Physics*, *118*, 6618–6626, doi:10.1002/jgra.50578.
- Heki, K., and Y. Enomoto (2014), Reply to comment by K. Heki and Y. Enomoto on "Preseismic ionospheric electron enhancements revisited", *J. Geophys. Res. Space Physics*, *119*, 6016–6018, doi:10.1002/2014JA020223.
- Kakinami, Y., M. Kamogawa, Y. Tanioka, S. Watanabe, A. R. Gusman, J.-Y. Liu, Y. Watanabe, and T. Mogi (2012), Tsunamiogenic ionospheric hole, *Geophys. Res. Lett.*, *39*, L00G27, doi:10.1029/2011GL050159.
- Kamogawa, M., and Y. Kakinami (2013), Is an ionospheric electron enhancement preceding the 2011 Tohoku-oki earthquake a precursor?, *J. Geophys. Res. Space Physics*, *118*, 1–4, doi:10.1002/jgra.50118.
- Kato, N. (2009), A possible explanation for difference in stress drop between intraplate and interplate earthquakes, *Geophys. Res. Lett.*, *36*, L23311, doi:10.1029/2009GL040985.
- Kuo, C. L., L. C. Lee, and J. D. Huba (2014), An improved coupling model for the lithosphere-atmosphere-ionosphere system, *J. Geophys. Res. Space Physics*, *119*, 3189–3205, doi:10.1002/2013JA019392.
- Maeda, J., and K. Heki (2014), Two-dimensional observations of mid-latitude sporadic-*E* irregularities with a dense GPS array in Japan, *Radio Sci.*, *49*, 28–35, doi:10.1002/2013RS005295.
- Maeda, J., and K. Heki (2015), Morphology and dynamics of daytime mid-latitude sporadic-*E* patches revealed by GPS total electron content observations in Japan, *Earth Planets Space*, *67*, 89, doi:10.1186/s40623-015-0257-4.
- Mannucci, A. J., B. D. Wilson, D. N. Yuan, C. H. Ho, U. J. Lindqwister, and T. F. Runge (1998), A global mapping technique for GPS derived ionospheric total electron content measurements, *Radio Sci.*, *33*, 565–582, doi:10.1029/97RS02707.
- Masci, F., J. N. Thomas, F. Villani, J. A. Secan, and N. Rivera (2015), On the onset of ionospheric precursors 40 min before strong earthquakes, *J. Geophys. Res. Space Physics*, *120*, 1383–1393, doi:10.1002/2014JA020822.
- Meng, L., J.-P. Ampuero, J. Stock, Z. Duputel, Y. Luo, and V. C. Tsai (2012), Earthquake in a maze: Compressional rupture branching during the 2012 M_w 8.6 Sumatra earthquake, *Science*, *337*, 724–726.

- Meng, L., H. Huang, R. Bürgmann, J. P. Ampuero, and A. Stader (2015), Dual megathrust slip behaviors of the 2014 Iquique earthquake sequence, *Earth Planet. Sci. Lett.*, *411*, 177–187.
- Nishimura, T. (2014), Short-term slow slip events along the Ryukyu trench, southwestern Japan, observed by continuous GNSS, *Prog. Earth Planet. Sci.*, *1*, 22, doi:10.1186/s40645-014-0022-5.
- Nishimura, T., T. Matsuzawa, and K. Obara (2013), Detection of short-term slow slip events along the Nankai Trough, southwest Japan, using GNSS data, *J. Geophys. Res. Solid Earth*, *118*, 3112–3125, doi:10.1002/jgrb.50222.
- Rideout, W., and A. Coster (2006), Automated GPS processing for global total electron content data, *GPS Solutions*, *10*, 219–228.
- Sakai, T. (2005), Bias error calibration for observing ionosphere by GPS network [in Japanese], *J. Inst. Electron. Inf. Commun. Eng.*, *J88-B*, 2382–2389.
- Shinagawa, H., T. Tsugawa, M. Matsumura, T. Iyemori, A. Saito, T. Maruyama, H. Jin, M. Nishioka, and Y. Otsuka (2013), Two-dimensional simulation of ionospheric variations in the vicinity of the epicenter of the Tohoku-Oki earthquake on 11 March 2011, *Geophys. Res. Lett.*, *40*, 5009–5013, doi:10.1002/2013GL057627.
- Tanioka, Y., L. Ruff, and K. Satake (1995), The great Kurile earthquake of October 4, 1994 tore the slab, *Geophys. Res. Lett.*, *22*, 1661–1664, doi:10.1029/95GL01656.
- Tsugawa, T., A. Saito, and Y. Otsuka (2004), A statistical study of large-scale traveling ionospheric disturbances using the GPS network in Japan, *J. Geophys. Res.*, *109*, A06302, doi:10.1029/2003JA010302.
- Utada, H., and H. Shimizu (2014), Comment on "Preseismic ionospheric electron enhancements revisited" by K. Heki and Y. Enomoto, *J. Geophys. Res. Space Physics*, *119*, 6011–6015, doi:10.1002/2014JA020044.
- Utada, H., H. Shimizu, T. Ogawa, T. Maeda, T. Furumura, T. Yamamoto, N. Yamazaki, Y. Yoshitake, and S. Nagamachi (2011), Geomagnetic field changes in response to the 2011 off the Pacific Coast of Tohoku earthquake and tsunami, *Earth Planet. Sci. Lett.*, *311*, 11–27, doi:10.1016/j.epsl.2011.09.036.